scientific reports

Check for updates

OPEN

Compatibility of fast tissue clearing with targeted fluorescence imaging and pathology analysis using clinical head and neck cancer biopsies

Ali Fakhrolmobasheri[1,6], Thomas S. Nijboer[2,6], Bas Keizers[3,4], Rozemarijn M. Kooij[1], Bert van der Vegt[5], Max J. H. Witjes[2], Floris J. Voskuil[2] & Pieter J. van der Zaag[1,3✉]

Complete tumor removal is crucial for successful surgical oncological outcomes. Targeted fluorescence imaging facilitates differentiation between healthy and cancerous tissue, enabling intraoperative margin assessment. However, its depth specificity is still limited. Three-dimensional fluorescence imaging could improve margin assessment, especially after tissue clearing. Conventional tissue clearing may take up to 24 h, limiting clinical applicability. This study developed and validated a *fast tissue clearing* protocol, achieving transparency within one hour. Ten patients from a fluorescence-guided surgery trial were included, from whom three tumor and three healthy tissue biopsies were acquired. These biopsies were used as control, cleared using a standard Benzyl Alcohol Benzyl Benzoate (BABB) clearing protocol, or cleared using the newly developed fast BABB clearing protocol. This protocol uses an orbital shaker, decreasing total process time to one hour. No significant difference in transparency was observed between normal and fast cleared biopsies. Fluorescence signals of all cleared biopsies increased directly after clearing and slowly decreased back to pre-cleared fluorescence signals over time. In non-cleared tumor biopsies, fluorescence intensity decreased substantially upon fixation, yet remained stable. Finally, clearing did not impact immunohistochemical staining. Therefore, fast tissue clearing is possible within one hour, enabling optical microscopy after tissue clearing for intraoperative pathology-assisted surgery.

During surgical removal of tumor tissue, the target for a successful oncological outcome is obtaining a tumor-free resection margin, i.e. no tumor present at the border of the resected tissue specimen, as assessed by pathology[1,2]. Tumor-positive margins decrease disease-free survival, highlighting the clinical relevance of tumor-free resection margins. This decrease necessitates adjuvant therapy, such as additional surgery, chemotherapy or radiotherapy[3–5]. Yet, between tumor types the clinical definition of a tumor-free resection margin differs. For example, in breast cancer surgery, a tumor-free margin is defined as no tumor at the resection margin, whereas a rim of at least 5 mm healthy tissue surrounding the tumor is recommended for head and neck cancer (HNC), while for vulvar cancer the guidelines advise margins of 8 mm[6–8].

[1]Molecular Biophysics, Zernike Institute, University of Groningen, 9747 AG Groningen, The Netherlands. [2]Department of Oral and Maxillofacial Surgery, University Medical Center Groningen, University of Groningen, 9713 GZ Groningen, The Netherlands. [3]Department of Nuclear Medicine and Molecular Imaging, University Medical Center Groningen, University of Groningen, 9713 GZ Groningen, The Netherlands. [4]Department of Surgery, University Medical Center Groningen, University of Groningen, 9713 GZ Groningen, The Netherlands. [5]Department of Pathology and Medical Biology, University of Groningen, University Medical Center Groningen, 9713 GZ Groningen, The Netherlands. [6]These authors contributed equally: Ali Fakhrolmobasheri and Thomas S. Nijboer. ✉email: p.j.van.der.zaag@rug.nl

Despite the necessity for obtaining tumor-free resection margins, current intraoperative assessment of margins only consists of tactile and visual inspection by the surgeon. Hence, a considerable number of surgeries show tumor-positive margins, ranging from 4.3% to 35.0% for the top ten most common cancer types in the United States[9]. To date, intraoperative fresh frozen sectioning is the commonly used technique to provide real-time margin feedback. However, this technique suffers from sampling errors, thus reducing sensitivity[10–12]. Recently, fluorescence imaging has emerged as an aid for surgeons to visualize tumors and resection margins intraoperatively. Both targeted and non-targeted fluorescent tracers are being evaluated. The last decade, especially targeted two-dimensional (2D) fluorescence imaging (FI) implemented in fluorescence-guided surgery (FGS) has shown great potential for laterally discriminating healthy from cancerous tissue, thereby enabling intraoperative margin assessment[13–21]. Nevertheless, accurate evaluation of margins remains challenging, notably for tumors requiring a healthy tissue margin. This is due to difficulty in localizing fluorescence signals in depth, due to scattering and the not 100% specificity of tracer binding. Sensitivity seems to be adequate for detecting tumor-positive margins (e.g. for HNC: tumor present within 1 mm of the resection edge), but is still inadequate for tumor involvement at the resection border covered by a couple of millimeters healthy tissue (e.g. the case of so-called close margins between 1 and 5 mm in HNC)[20]. A strategy to improve margin assessment using FI, could be through increased visualization of the fluorescently labeled cancer cells in margins of the resection specimen through optical microscopy techniques, such as confocal laser scanning microscopy (CLSM) and light-sheet fluorescence microscopy (LSFM). These techniques enable back-table assessment, such that the pathologist can provide real-time margin information, i.e. intraoperative pathology assessment, that can serve as a diagnostic tool during surgery[22]. LSFM achieves fast imaging speeds of large samples (1 mm^3/min)[23]. Yet, for LSFM to work, the light penetration into the tissue should be improved as this still is a limiting factor[22,24].
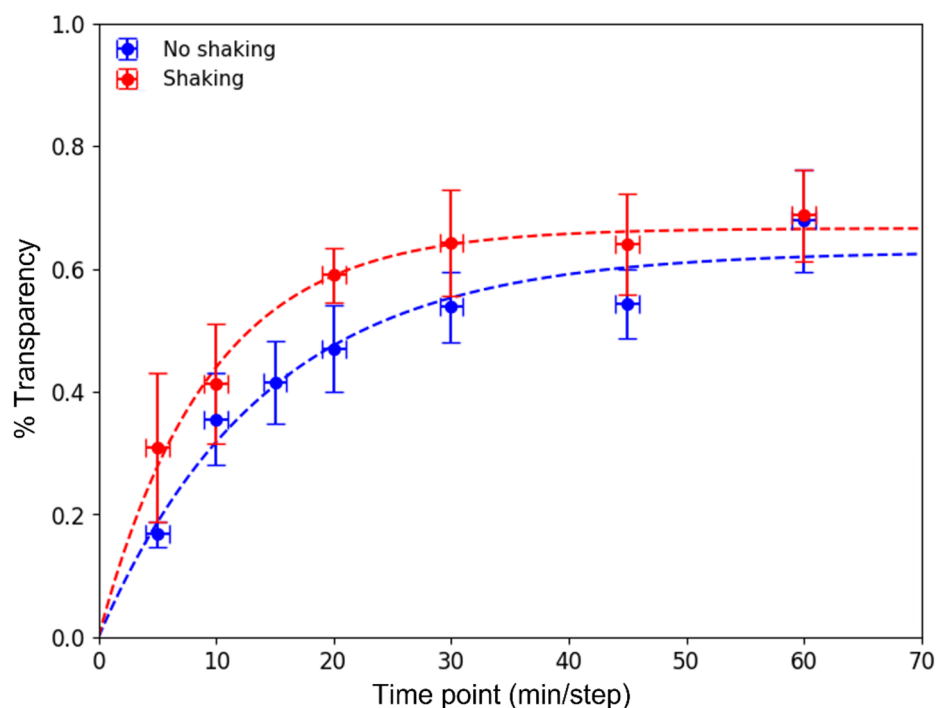
Light scattering is the main cause for the limited light penetration depth and consequently limits the use of microscopy techniques in tissue analysis. Tissue clearing reduces light scattering by matching the refractive index of the tissue components[25]. Hence, tissue clearing is a potential solution to overcome this limitation of LSFM and CLSM, which would then enable detection of fluorescence targets at greater depths. Tissue clearing in combination with these high-resolution or super-resolution microscopy techniques, facilitates 3D visualization of complex biological systems and cellular structures, e.g., the tumor environment[26–28]. Despite recent advances, tissue clearing remains a relatively slow technique, typically requiring several hours to complete[25,29]. A study has reported to clear a sample within an hour, yet the distance cleared was limited to ≤ 100 μm[30]. Generally, biopsies and resection margin require assessment and thus clearing of over greater depths of a few (3–5) mm. Among tissue clearing methods, the solvent-based method is regarded as one of the most effective tissue-clearing techniques. Amongst the first and most efficient protocols in this category is the Benzyl Alcohol Benzyl Benzoate (BABB) method[25]. This approach utilizes a hydrophobic agent for refractive index (RI) matching, necessitating an initial dehydration step to replace water with an alcohol, e.g. methanol. The dehydration process strongly relies on osmotic pressure. Therefore, the diffusion time can be minimized by applying increased pressure during this step[25,31,32]. For intraoperative pathology-assisted surgery to be feasible, tissue clearing over millimeter distances should be achieved within approximately one hour. For HNC, lymph node removal (via sentinel node biopsy or neck dissection) is part of the standard of care surgical procedure and typically takes one to four hours, depending on extensiveness. While this step normally precedes tumor removal, reversing this sequence creates a time window to clear and image tissue. However, before performing a clinical trial proving the benefit of clearing in FGS, tissue clearing must be proven to not hamper conventional pathology assessment nor the fluorescence from the optical contrast agents, needed to perform FGS. Therefore, the aim of the current study was to develop a so-called *fast tissue clearing* protocol, clearing within a clinically relevant time frame (i.e. one hour) and to investigate its compatibility with standard pathology processing and current FGS requirements. This protocol will be compared to conventional BABB clearing (protocol based on[33]) in terms of level of transparency, influence on tracer fluorescence intensities and tissue integrity. Influence on tracer fluorescence intensities will be monitored in this study, as tissue clearing has not been combined with targeted fluorescence imaging of human tissues before. For the current proof-of-concept study, tumor and healthy tissue samples of HNC patients, who participate in a clinical fluorescence-guided surgery trial, were used[4].
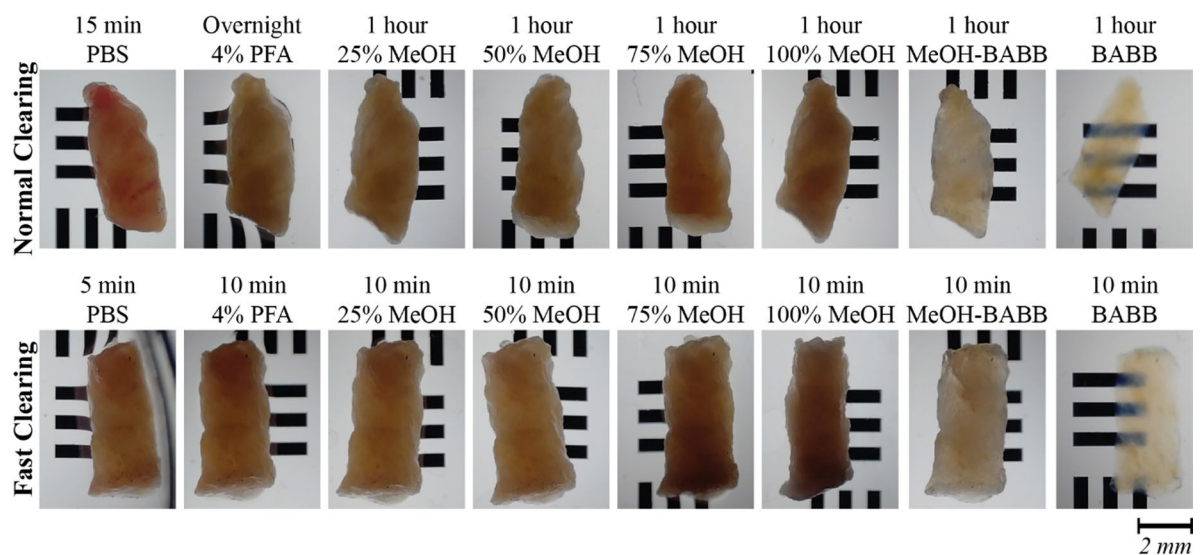
Results
Transparency
To speed up the tissue clearing process, we explored using turbulence by the introduction of an orbital shaker in the protocol (see Sect. 5. Material and Methods) and reducing each process step in conventional BABB tissue clearing from 1 h to 10 min, or below for the phosphate buffered (PBS) washing step. Figure 1 shows how, for 4 mm biopsies obtained from pig tongue, the transparency varies as a function of process step duration. The curve through the data is a fit to an exponential dependence. This fit yields a time constant τ of 14.1 ± 2.2 min per step. This value is in line with the diffusion times and constants we have found for BABB in other tissues[34]. Upon adding shaking to the protocol the tissue clearing process speeds up and τ becomes 9.3 ± 0.8 min per step. These data show that a clearing protocol using 10 min process steps yields a transparency adequate for analysis, while for 5 min process steps the transparency is reduced to 30%, inadequate for analysis. This is illustrated in Fig. 2. Here, a representative example of the normal BABB and the newly conceived fast clearing process are shown for ~ 2 × 2 × 5 mm^3 biopsies, including the time used for each process step.

As the main goal of the tissue clearing process is to make samples transparent for 3D fluorescence imaging, the effect of the fast and normal tissue clearing protocols on the achieved transparency T was determined. For this analysis, clinical biopsies with and without the fluorescent tracer cetuximab-IRDye800CW were used. As shown in Fig. 3A, for both tumor and healthy tissue, a median transparency of above 75% was achieved, without a statistical difference between fast and normal clearing. A median transparency of 81.6% (standard deviation (SD) = 13.0%) was acquired for the *fast* clearing of tumor tissue, compared to 82.5% (SD = 14.6%) for

Fig. 1. Transparency of pig tongue tissue for different processing time steps. Transparency obtained with shaking (red) and without shaking (blue) is plotted as a function of the duration of each clearing step. For details, see text.
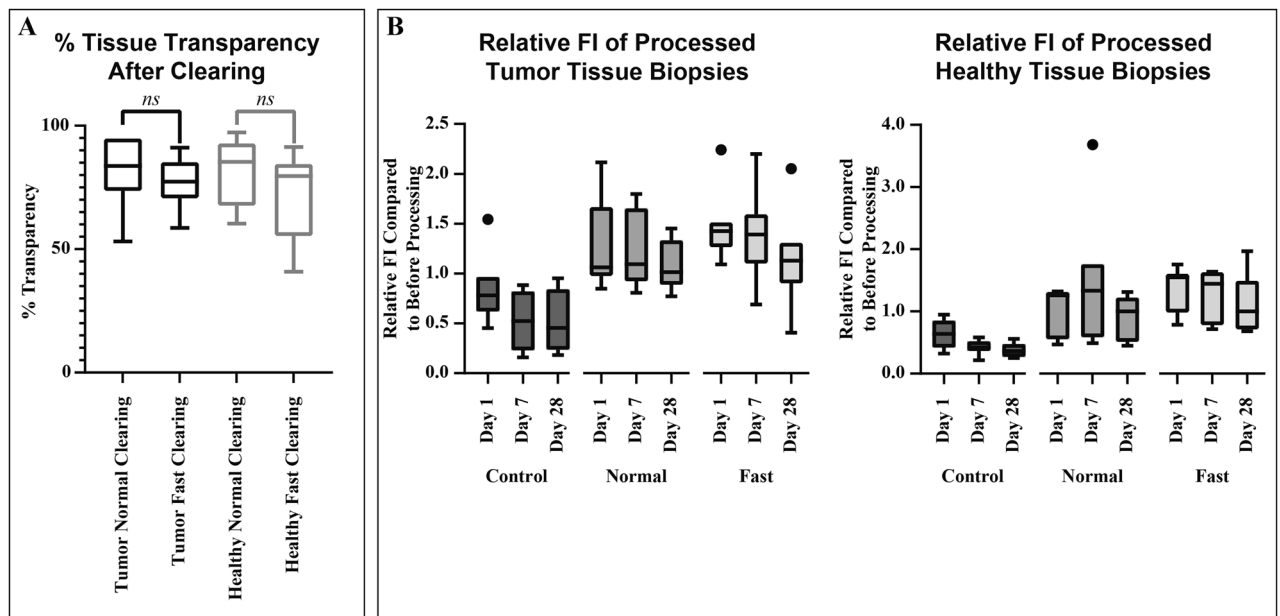

Fig. 2. White light images of head and neck cancer tumor biopsies for each of the eight clearing process steps. The top and bottom rows show normal and fast clearing protocols, respectively. The time duration of each step is indicated: total time for normal and fast clearing is 18 h and 75 min, respectively. Abbreviations: Phosphate-buffered saline (PBS), Paraformaldehyde (PFA), Methanol (MeOH), Benzyl Alcohol Benzyl Benzoate (BABB).

normal clearing of tumor tissue. A similar result was found for healthy tissue: 78.2% (SD = 17.2%) and 81.9% (SD = 10.5%) for fast and normal clearing, respectively.

Fluorescence imaging

To compare the effect of normal and fast clearing protocols on fluorescence imaging, 2D fluorescence imaging was performed before clearing, as well as 1, 7 and 28 days after clearing. Figure 3B shows changes in fluorescence

Fig. 3. Quantitative analysis of tissue clearing effects. (**A**) Boxplots with median, interquartile range (IQR), minimum and maximum, showing the achieved transparency of both the tumor and healthy samples, including samples with and without tracer, for both tissue clearing protocols. Abbreviations: no significant difference (ns). (**B**) Boxplots with median, IQR, minimum and maximum measured fluorescence intensities (FI) relative to before clearing over a 28-day time period for the three approaches investigated: normal and fast clearing and a control. The solid dots represent outliers.

intensities, relative to before clearing, for both tumor and healthy tissue biopsies. As shown, clearing increased the median fluorescence intensity of tumor tissue by 43% (IQR = 18%) and 6% (IQR = 45%), for fast and normal clearing, respectively. For healthy tissue, intensity increased by 55% (IQR = 45%) and 26% (46%), respectively. Intensities of control biopsies decreased by 12% (IQR = 29%) and 36% (38%) for tumor and healthy tissue, respectively. Overall, the intensities of cleared biopsies show some, but limited, decay. No significant differences in fluorescence intensities were found when comparing the fast and normal clearing protocols. However, fluorescence signals in control biopsies were significantly lower for tumor tissue compared to fast ($p < 0.0001$) and normal clearing ($p = 0.002$) as well as for healthy tissue ($p < 0.0001$ and $p = 0.004$ for fast and normal clearing, respectively). Figure 4 shows representative images of biopsies taken from a single patient in white light, 2D fluorescence and 3D fluorescence, respectively. Figure 4 shows influence of clearing on transparency (white light images, columns 1–2), change in fluorescence patterns over time before and after clearing (2D fluorescence images, columns 3–5), and the possibility to perform microscopy analysis using confocal microscopy (3D fluorescence images, column 6).
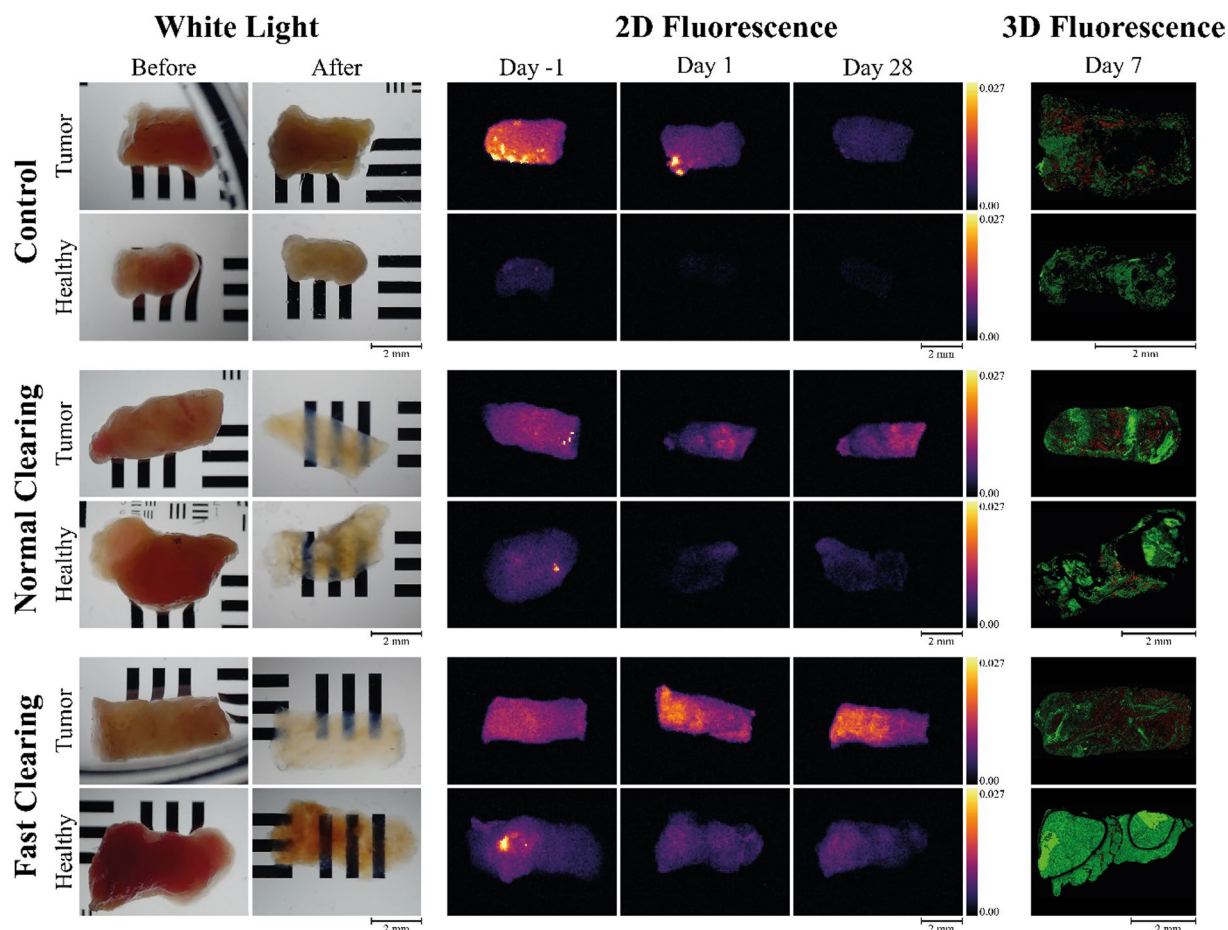
The data of 3D confocal fluorescence imaging shows that the imaging depth in non-cleared samples is restricted to only 150 µm. In contrast, cleared tissue samples could be imaged up to 750 µm depth, limited by the confocal objective. Imaging the sample from 2 sides, enabled imaging of up to 1.5 mm into the tissue. Figure 5 highlights the difference between conventional fluorescence imaging, before clearing, and confocal fluorescence microscopy, after fast tissue clearing, in more detail. For this, a z-stack of the sample was made by confocal microscopy. Example videos of these z-stack images, i.e. 3D visualization, are shown in the supplementary information. In Fig. 5, the confocal image shows a cross-section at a depth of 600 µm, with an overall transparency of 61%. In the conventional fluorescence image, tracer can be localized, however exactly pinpointing dye location remains challenging. Yet, from the 3D confocal image, tracer signals can accurately be located within the tissue, enabling evaluation of in-patient tracer distribution on a cellular level.

During this trial, we had the opportunity to acquire complete fresh tissue slices to investigate the possibility of fast clearing larger samples. For comparison, this tissue slice was cut in half, so it could be cleared using the normal and fast protocol. Again, no differences between both clearing protocols were observed and performing hematoxylin and eosin (H&E) staining of the tissue section was still feasible.
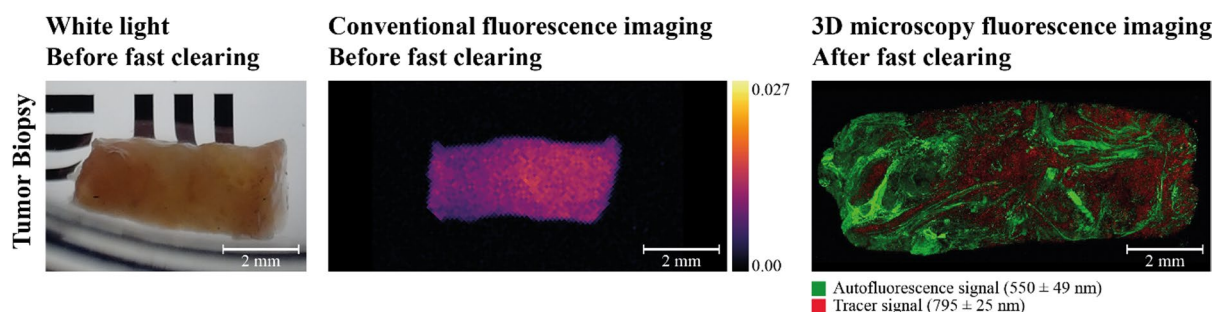
H&E and immunohistochemistry staining

H&E and immunohistochemistry (IHC) staining was performed on all tumor biopsies. Tissue clearing did not hamper pathology assessment of the H&E and IHC staining. The staining was comparable between the different methods (fast clearing, normal clearing and control). Visually, no artefacts could be detected and the membranous staining cytokeratin AE1/3 (CK AE1/3) and epidermal growth factor receptor (EGFR) clearly showed a strong membranous coloring. Furthermore, programmed death-ligand 1(PD-L1) staining showed an expected staining pattern, indicating the possibility to apply this staining after clearing. Representative examples of the staining are shown in Fig. 6.
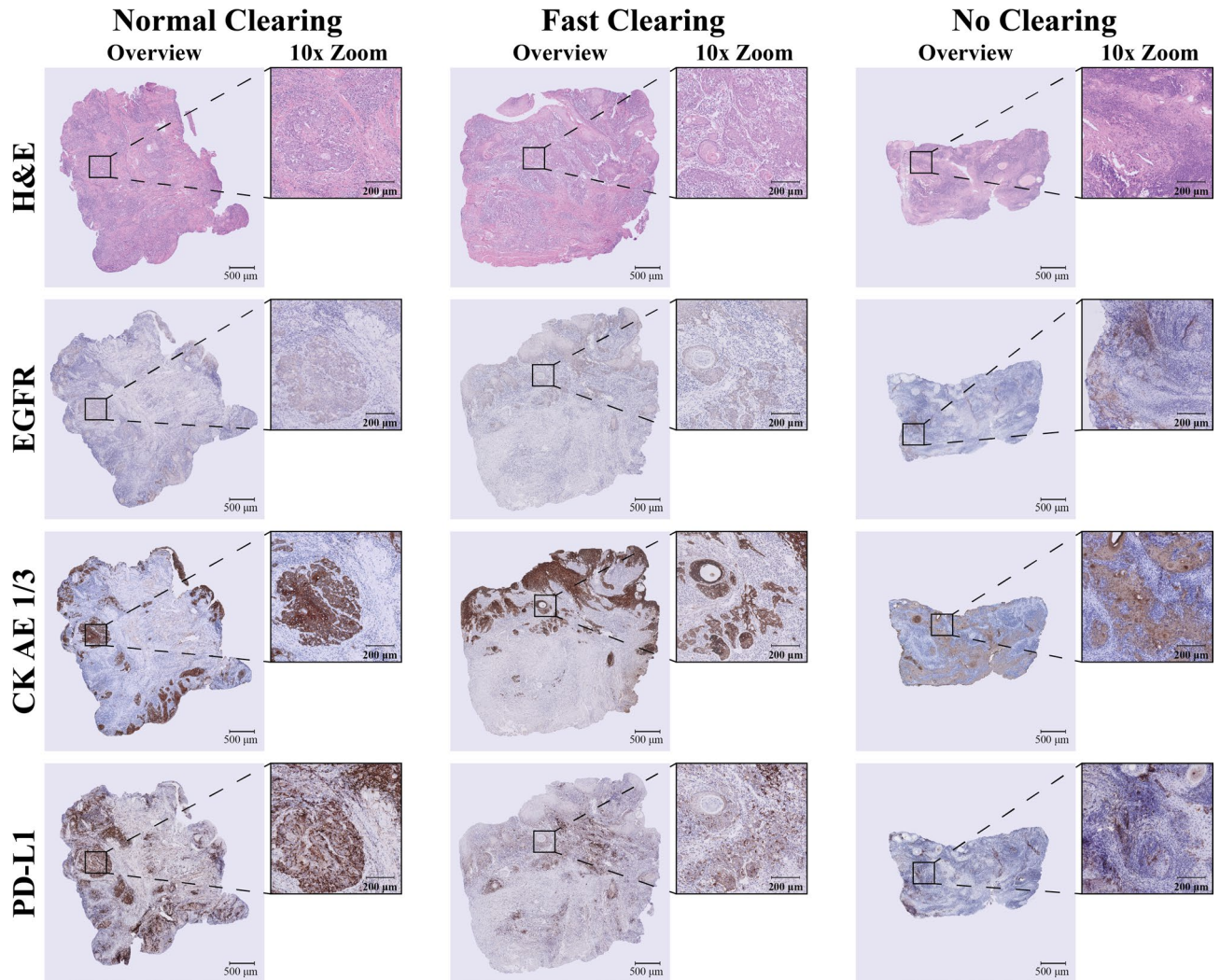
Fig. 4. Overview of representative examples of fluorescence images obtained for control, not cleared, (top 2 rows), normal cleared (middle 2 rows) and fast cleared biopsies (bottom 2 rows). For each clearing approach both tumor tissue, containing the fluorescent tracer, and healthy tissue, obtained from the same patient, were analyzed. Column 3–5 show images obtained with the fluorescence imaging system at different time points: before, 1 and 28 days after tissue clearing. The 6th column shows the confocal imaging results 7 days after clearing.

Fig. 5. Highlight showing the comparison between conventional fluorescence imaging and 3-dimensional (3D) confocal microscopy imaging following fast tissue clearing. For conventional fluorescence imaging, a detecting wavelength of 800 nm was used. For the 3D microscopy image, autofluorescence (green) channel was excited at 488 nm and detected at 550 ± 49 nm. The fluorescent tracer (red) channel was excited at 765 nm and detected at 795 ± 25 nm. Videos of additional 3D confocal microscopy examples are shown in the supplementary information.

Fig. 6. Representative examples of the hematoxylin and eosin (H&E), epidermal growth factor receptor (EGFR), cytokeratin AE1/3 (CK AE1/3) and programmed death-ligand 1 (PD-L1) staining of 4 µm tissue sections for a normal and fast cleared tumor biopsy and a control (not cleared) biopsy.

Discussion

To date, no studies have been performed investigating the combination of tissue clearing within an hour and FGS. Therefore, this study aimed to develop a fast clearing method to assess tumor tissue within an hour, that is compatible with FGS and without hampering regular histopathology assessment, such a method would enable the optimizing of intraoperative margin assessment through fluorescence imaging. Our newly developed protocol is an optimized BABB-based protocol for which each process step was reduced to ten minutes, as this time represents an optimal balance between clearing efficiency and time (Fig. 1). This fast-clearing protocol was compared to the normal, 6-hour, BABB clearing protocol[33] in terms of transparency, fluorescent tracer stability and pathology assessment. Overall, no difference between the fast and normal clearing protocol was found for any of the investigated criteria. Therefore, fast tissue clearing could improve tumor margin visualization by using high-resolution 3D microscopy and may enable intraoperative pathology-assisted surgery and intraoperative correction of inadequate resection margins[22].

Samples originating from various parts of the oral cavity were used in this study (see Sect. 5.1), and without any difference in transparency observed between them. This result is consistent with a recent study showing that the diffusion constant in the BABB tissue-clearing process does not vary significantly across different tissue types[34]. A comparable transparency is obtained for both normal and fast clearing, with a total time after fixation of 6 h and 1 h, respectively, indicating the possibility to employ the fast clearing protocol as an alternative to the normal clearing protocol to clear tissue biopsies (Fig. 3A). Since the obtained transparency of both protocols is consistent with prior findings, this demonstrates the possibility to use BABB-based clearing to enhance tissue transparency[35,36]. Also, compared to previous studies attempting tissue clearing in one hour, we are able to clear larger tissue samples (100 µm in literature versus 4 mm in our study)[30]. Next, an important aspect to analyze in these tissue clearing experiments is the compatibility of clearing with targeted FI, especially for the clinically applicable fast clearing protocol in FGS[37,38]. In this study, samples from seven patients contained the targeted

fluorescent tracer cetuximab-IRDye800CW. A progressive increase in fluorescence intensity was found after tissue clearing (Fig. 3). This may be the result of a reduction in light scattering owing to tissue clearing, enabling deeper tissue penetration of the excitation light, exciting more optical contrast agents, resulting in the factor 1.5 increase in fluorescence detected. As can be seen in Fig. 4, obvious fluorescence signals are visible in the healthy tissue biopsies before clearing. These clear fluorescence signals were removed upon clearing. These signals are probably caused by unbound tracer present in tumor surroundings, flushed away during tissue clearing. Fluorescence signals remained stable during the following 28-day period. This period is well in excess of the time needed for intraoperative FGS (approx. 1 h). These results align with previous studies highlighting the prolonged stability of fluorescence signals in cleared tissues[39]. The decay in fluorescence in the control sample can be understood to occur owing to the molecular oxygen insertion into the C–H bond of aldehyde group in formalin leading to decomposition of IRDye800CW[40,41]. Finally, both normal and fast clearing did not influence H&E and IHC assessment for CK AE 1/3, EGFR and PD-L1 on 4 μm tissue sections, consistent with previous studies[25,31]. Fig. 6 shows that the EGFR staining appears weaker, compared to CK AE1/3 and PD-L1 stainings. This is due to the inherent heterogeneity of these biomarkers in tumors, as a board-certified pathologist did not consider the cleared samples to be different from the control samples (third column in Fig. 6). Consequently, in this study we showed compatibility of the proposed fast clearing protocol with FI, while still being able to perform standard histopathology assessment.

Besides these promising results, some considerations remain. First, fast clearing biopsies of two patients were cleared twice using the fast clearing protocol. After the first fast clearing procedure, these biopsies did not become transparent in the allotted time, due to failure of the orbital shaker. As the BABB clearing process enables clearing reversal by performing the process in reverse (up to the fixation step), the biopsies were uncleared and cleared again using the fast clearing protocol. After this additional procedure, no differences in achieved transparency and fluorescence were observed compared to the other fast cleared biopsies. Accordingly, the influence of the clearing process is limited and tissues can be cleared and uncleared without hampering fluorescence imaging or pathology assessment. Second, only BABB clearing has been investigated, since solvent-based clearing methods, based on BABB or derived agents, play a dominant role in the tissue clearing field. New clearing techniques may arise, enabling faster and easier clearing[25,42]. Additionally, at the resection margin high intensity signals were detected using 3D confocal imaging. These signals could be attributed to the presence of pathology orientation ink. Even though this could easily be detected as an artefact, extra caution was taken to not include ink in the biopsy, resulting in biopsies not showing this artefact. Last, confocal imaging is generally considered a slow technique with limited tissue penetration. Therefore, using a light-sheet microscope would result in faster, and higher quality images[23].

These findings suggest that the fast tissue clearing protocol offers a viable and efficient method for enhancing both fluorescence imaging depth and intensity, thereby supporting its potential utility in clinical settings. Due to decreased light scattering, 3D imaging of up to 750 μm is possible, a depth that was limited by the confocal objective. In contrast, fluorescence signals in non-cleared control samples diminished significantly beyond 100 μm and were nearly undetectable at depths greater than 150 μm. Previous studies have utilized camera-based imaging systems, such as CMOS and CCD sensors, to image samples with near-infrared tracers to depths of several millimeters[13,43]. In contrast, the confocal imaging system excites the sample point by point, using a photon detection system to capture the images. Therefore, the difference in imaging depth can be attributed to the variation in imaging modalities. Similar trends in imaging depth have been observed in studies utilizing the confocal microscope and different optical clearing methods[39,44]. This was again confirmed by quantitative analysis of fluorescence signals. As shown in Fig. 3B, an increase in fluorescence intensity was detected for cleared tissue samples, whereas fixing the control biopsies diminished the fluorescence signal. Excitation light penetrates deeper into cleared tissue sample, thus exciting more fluorophores. Additionally, emission from more fluorophores penetrates through cleared tissue and thereby reaches the detector, increasing fluorescence intensity. Moreover, no complications arose in staining cleared samples, probably owing to the similar nature of the processes of dehydrating and fixing the samples for the BABB clearing and regular pathology fixation. Hence, tissue clearing seems a viable option to explore for easier application of fluorescence imaging in the clinical setting. Reinforced by an increased tumor distinction because of a decrease of unbound tracer in healthy, background, tissue and increase in fluorescence intensities in tumor tissue due to reduction of scattering. However, as of now, these findings are limited to biopsies only and the protocol should be investigated for its applicability in larger samples, i.e. resection specimens. In such a trial, investigating the colocalization of cetuximab and its target EGFR will be of great interest. In this current trial we were unable to maintain the orientation of the biopsies, inherent to their tubular shape. However, when clearing and imaging larger samples such as tissue slices or resection specimens, orientation tracking will be easier and colocalization can be investigated.

The tissues slices studied indicate the possibility to extrapolate the proposed fast clearing protocol to larger clinical samples. In the current study, only HNC samples were investigated, HNC being one of the cancers for which free tumor margin requirements are quite stringent. Further studies should explore the applicability of this protocol in other tissue types (e.g. tissues containing more fatty tissue, such as breast tissue). Additionally, it would be of great interest to investigate the propagation of clearing agents throughout the tissue while clearing, to get better insight in how tissue becomes clear over time to determine the exact clearing time required for specific samples[34]. Such understanding of the diffusion process may be used to improve clearing agent diffusion. Even though the fast clearing protocol enables clearing within an hour, this should ideally be reduced even further for rapid clinical implementation, as not all tumor removal surgeries facilitate a one to four hour time window for clearing and imaging. Further decrease of clearing time could be achieved by omitting redistributing the time amongst the four dehydration steps as well as adding stirring, but this needs to be investigated further. Finally, the realization that not necessarily the whole resection specimen needs to be cleared, but just the crucial edges is important to consider. Depending on cancer type, achieving a tumor-free margin of approximately

3–5 mm is generally required[24]. As edges clear considerably faster, focusing clearing on this critical margin may be particularly advantageous[34]. If the process of clearing and imaging could be reduced to less than an hour, using for example light sheet microscopy, this would allow for intraoperative pathology-assisted surgery and consequent reduction of inadequate margins[22]. This proof-of-principle study shows subsequent clinical trials can be designed to investigate the possibility to do tissue clearing of resection specimens within an hour combined with 3D fluorescence imaging to facilitate further optimization.

Conclusion

To conclude, we have reported a *fast*, BABB based, clearing protocol, yielding similar results compared to normal BABB clearing based on obtained transparency, compatibility with fluorescence imaging, and standard pathology assessment, for the first time. Fluorescence intensities remained stable over 28 days, well beyond what is needed clinically. Moreover, tissue clearing proved to be compatible with the IRDye800CW-based tracer used in targeted fluorescence-guided surgery as well as standard of care histopathology staining. Thus, fast tissue clearing appears to be well-suited for clinical samples, opening the possibility of using fast tissue clearing in combination with optical microscopy for intraoperative pathology-assisted surgery in clinical care.

Materials and methods

An overview of the protocol used is shown in Fig. 7. All steps of the process are described in more detail in the following sections.
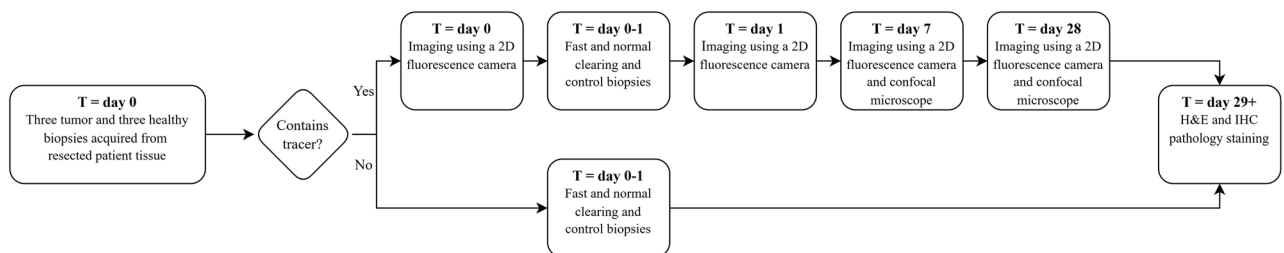
Sample collection and preparation

For clearing time measurements, pig tongue samples were purchased from a local slaughterhouse (Kroon Vlees, Groningen), frozen at -24 °C within 4 h, and stored frozen until use. Biopsies were taken from the frozen samples stored at -24 °C, using a 4 mm disposable biopsy punch (Robbins Instrument, Texas, USA). Clinical samples were collected from a trial investigating fluorescence imaging in patients with head and neck cancer (HNC), approved by the ethical review board of the UMC Groningen and executed in the University Medical Centre Groningen (UMCG) (clinincaltrials.gov: NCT05499065). Informed consent has been obtained from all patients. All research was conducted in accordance with the principles of the Declaration of Helsinki (adapted version of Fortaleza, Brazil, 2013). In this study, patients with HNC received a dose of 75 mg of the antibody cetuximab, followed by 15 mg fluorescence labelled cetuximab-IRDye800CW two days prior to standard of care surgery, according to study protocol and based on previous data[17,20]. Within 30 min after surgery, the excised tissue was freshly cut into 3–5 mm thick tissue slices at the Department of Pathology of the UMCG. From these tissue slices, three biopsies of macroscopically visible and palpable tumor and healthy tissue, acquired distant from the tumor, were obtained with a 4 mm biopsy puncher (Henke Sass Wolf, Tuttlingen, Germany) and assigned to either the new *fast clearing*, normal clearing or control protocol, as described hereafter. A board-certified pathologist assessed the biopsies and determined the healthy tissue biopsies did not contain any tumor tissue. For each protocol, one tumor and one healthy tissue biopsy were used per patient. As additional test, biopsies were acquired from HNC patients not participating in the previously described study, i.e. having no fluorescent tracer administrated. A declaration by the medical ethics committee that this study does not fall under the Dutch Act on Medical Research involving Human Subjects has been acquired. Fresh biopsies were obtained similarly. These biopsies were solely used to compare the fast and normal clearing protocol based on transparency and tissue integrity. In total, 60 biopsies from ten patients (6 biopsies per patient) were acquired: seven patients with a fluorescent tracer and three patients without. The biopsies containing the fluorescent tracer originated from tongue ($n = 5$), cheek ($n = 1$) and floor of the mouth ($n = 1$) tissue, and all biopsies without fluorescence tracer originated from tongue tissue ($n = 3$).

If clinically possible, as deemed by a board-certified head and neck pathologist, a single tissue slice was also obtained for study purposes. Such a tissue slice was subsequently cut in half. Each half was either cleared using the *fast* or the normal clearing protocol.

Tissue sample imaging

Biopsies containing the fluorescent tracer, were imaged with two setups: a wide-field fluorescence camera imaging system and confocal microscope. Wide-field fluorescence imaging of the biopsies was performed with

Fig. 7. Overview of study protocol including time-points of imaging, clearing and pathology staining: hematoxylin and eosin (H&E) staining and, immunohistochemistry (IHC) staining (epidermal growth factor receptor, cytokeratin AE1/3 and programmed death-ligand 1).

a closed-field imaging system using the 800 nm channel (PEARL Trilogy, LI-COR, NE, USA). Two-dimensional macroscopic fluorescence imaging was performed prior to clearing, and 1, 7 and 28 days after clearing. Fluorescence intensities were recorded as counts given by this system as is common practice in FGS trials[17,45]. To compare fluorescence signals over time, the mean fluorescence intensity of each biopsy was evaluated relative to its baseline value (before clearing of the corresponding biopsy). These values are given as the relative fluorescence intensity.

For three-dimensional (3D) fluorescence imaging of the tissue samples, confocal laser scanning microscopy (CSLM) was performed, via a confocal microscope (STELLARIS 8, Leica, Germany), equipped with a 10× objective lens (HC PL APO 10x/0,40 CS2, Leica, Germany). In CLSM, two channels were employed for image capturing: an excitation wavelength of 765 nm and detection wavelength of 795 ± 25 nm for imaging the fluorescent tracer. For imaging the autofluorescence an excitation wavelength of 488 nm and detection wavelength of 550 ± 49 nm was used. A z-stack with 20 μm steps was used. Imaging with the confocal microscope was performed at day 7 and 28. Data were collected and analyzed using dedicated analysis software (Leica Application Suite X (LAS X), version 4.8.2.29567, Leica Microsystems, Wetzlar, Germany).

Tissue clearing

BABB clearing was used since this is the first and most common hydrophobic clearing method, owing to its excellent clearing properties[25,33,35]. To improve the diffusion speed of agents in the tissue clearing process, the use of an orbital shaker (VWR™ Standard 1000 Standard Orbital Shaker) was introduced. To generate the data presented in Fig. 1, the following protocol was applied. The duration of each step was determined according to specific time points after the fixation step (5, 10, 15, 20, 30, 45, and 60 min). For each time point, the experiment was performed twice: once with shaking and once without shaking.

I.   Washing the samples for 5 min in PBS (Sigma-Aldrich, P4417).
II. Sample fixation in 4% formaldehyde (Sigma-Aldrich, 1.00496) for 10 min.
III. Dehydrating the samples with graded methanol wash (MeOH, Macron Fine Chemicals), starting at 25% and increasing by 25% at each step up to 100% solvent. Graded methanol was produced using a mixture of methanol and Milli-Q water (v: v).
IV. Matching RI of the samples by submerging them in a 1:1 (v: v) mixture of 100% MeOH and 100% BABB (a 2:1 (v: v) mixture of benzyl benzoate (Sigma Aldrich, Saint Louis, USA) and benzyl alcohol (Sigma Aldrich, Saint Louis, USA)), and subsequently in 100% BABB.

Each incubation step was carried out based on the time points. Based on this, two protocols were derived from the BABB clearing protocol[33], based on clearing time: A normal BABB clearing protocol and the newly developed *fast clearing* protocol with clearing times of 6 h and 1 h, respectively. The samples were placed in petri dishes during tissue clearing. Clearing was performed at room temperature for both protocols. Clearing steps are described below (see Fig. 2).

Normal BABB clearing:

I.   Washing samples for 15 min in Phosphate buffered saline (PBS) (Sigma-Aldrich, P4417).
II. Overnight sample fixation in 4% formaldehyde (Sigma-Aldrich, 1.00496).
III. Dehydrating the samples with graded methanol wash (MeOH, Macron Fine Chemicals), starting at 25% and increasing by 25% at each step up to 100% solvent. Graded methanol was produced using a mixture of methanol and Milli-Q water (v: v).
IV. Matching Refractive index (RI) of the samples by submerging them in a 1:1 (v: v) mixture of 100% MeOH and 100% BABB (a 2:1 (v: v) mixture of benzyl benzoate (Sigma Aldrich, Saint Louis, USA) and benzyl alcohol (Sigma Aldrich, Saint Louis, USA)), and subsequently in 100% BABB.
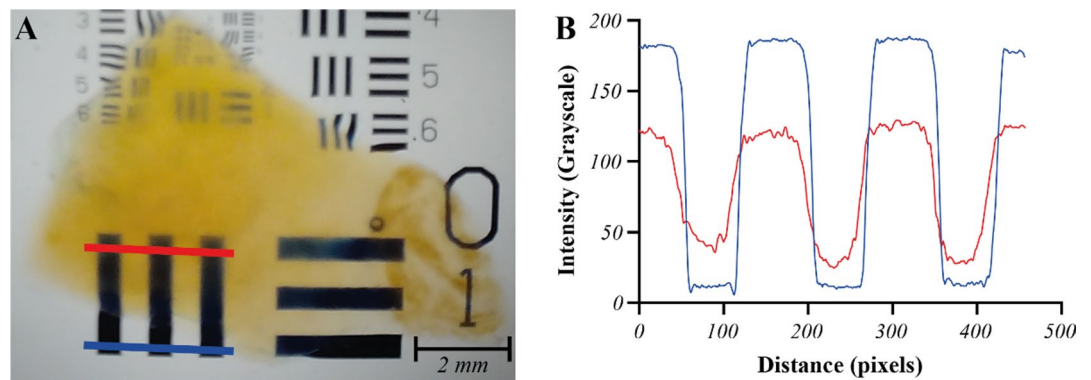
Each incubation step in III is carried out for 1 h[33,36]. ; together with step IV, the total clearing process duration after fixation is 6 h.

Fast BABB clearing:

To decrease the diffusion time and thereby clearing time, an orbital shaker (VWR® Standard 1000 Standard Orbital Shaker) at 200 rpm was used in the following protocol for all steps:

I.   Washing the samples for 5 min in PBS.
II. Sample fixation in 4% formaldehyde for 10 min.
III. Dehydrating the samples with graded methanol wash (MeOH, Macron Fine Chemicals), starting at 25% and increasing by 25% at each step up to 100% solvent. Graded methanol was produced using a mixture of methanol and Milli-Q water (v: v).
IV. Matching RI of the samples by submerging them in a 1:1 (v: v) mixture of 100% MeOH and 100% BABB (a 2:1 (v: v) mixture of benzyl benzoate (Sigma Aldrich, Saint Louis, USA) and benzyl alcohol (Sigma Aldrich, Saint Louis, USA)), and subsequently in 100% BABB.

Each incubation step in III was carried out for 10 min; together with step IV, the total clearing process duration after fixation is 1 h.

                9

Fig. 8. Example of the transparency measurement. (A) Shows the tissue of interest on a 1951 USAF target. The sample was cleared using the fast clearing protocol, reaching a transparency of about 75%. A region of interest was selected outside the tissue (blue line) and within the tissue (red line). (B) shows intensity plots along the lines outside the tissue (blue profile) and within the sample tissue (red profile).

Transparency measurements

To examine the influence of clearing in terms of transparency, all samples were imaged using a standard microscope (UltraZoom Pro Digital microscope, dnt Innovation GmbH, Leer, Germany) before clearing and directly after clearing with the BABB solvent. The tissue of interest was imaged on a 1951 USAF target (Edmund Optics, 38–257, NJ, USA). In this image, a region of interest (ROI) was selected within the tissue. Using ImageJ (version 1.54f, Fiji, Bethesda, MD, USA, https://imagej.net/software/fiji/downloads), a line was drawn through the ROI perpendicular to the light and dark stripes of the grating that were visible through the cleared tissue (Fig. 8A, red line). Similarly, another line was drawn outside the tissue (Fig. 8A, blue line) for comparison.

The average pixel intensity within the ROIs was used to calculate the average Michelson contrast in the image, C, using [26]

$$C = \frac{I_{max} - I_{min}}{I_{max} + I_{min}}, \tag{1}$$

with I_{max} being the maximum intensity (light part of grating) and I_{min} is the minimum intensity (dark part of grating) as shown in Fig. 8B.

The contrast of the grating was measured within the sample (C_{sample}) and outside the sample (C_{base}) to calculate the transparency (T), as

$$T = \frac{C_{sample}}{C_{base}}. \tag{2}$$

Microscopic assessment using conventional staining

In the final step, after imaging of the samples on day 28 had been completed, the tissue biopsies were formalin fixed, paraffin embedded and subsequently sectioned (4 µm) and hematoxylin and eosin (H&E) stained. Additionally, tissue sections were also stained for the epidermal growth factor receptor (EGFR.113, Monosan, 1:20), cytokeratin (CKAE1/3; PAN, Ventana, RTU) and programmed death-ligand 1 (PD-L1, 22C3, DAKO, 1:50) on an automated staining platform (Ventana Benchmark Ultra). These three stainings were chosen as these cover the key relevant targets for clinicians. For clinical applicability, all stained biopsies were assessed on quality by a board-certified pathologist, blinded to the type of clearing.

Data processing and statistical analysis

All raw image data were analyzed using ImageJ (version 1.54f, Fiji, Bethesda, MD, USA, https://imagej.net/software/fiji/downloads) and LAS X software (Leica Application Suite X (LAS X), version 4.8.2.29567, Leica Microsystems, Wetzlar, Germany). Data was subsequently analyzed in Excel (version 2410, Microsoft, Redmond, WA, USA) and GraphPad Prism (version 9.1.0, GraphPad Software Inc, San Diego, CA, USA). All data was considered non-normally distributed and statistical differences were tested using the Mann-Whitney test.

Data availability

Data used in this study are available upon reasonable request to the corresponding author. De-identified patient data will be available, as well as transparency and fluorescence data.

References

1. Slootweg, P. J., Hordijk, G. J., Schade, Y., Van Es, R. J. J. & Koole, R. Treatment failure and margin status in head and neck cancer. A critical view on the potential value of molecular pathology. *Oral Oncol.* 500–503. https://doi.org/10.1016/s1368-8375(01)00092-6 (2001).
2. Hafström, A., Wahlberg, P., Klasson, S., Greiff, L. & Sjövall, J. Predictors of survival in advanced oral cancers after salvage surgery with free tissue flap reconstruction. *Eur. Arch. Otorhinolaryngol.* **280**, 2953–2964 (2023).
3. Lee, D. H. et al. Close surgical margins in oral and oropharyngeal cancer: Do they impact prognosis? *Cancers (Basel)* **14**, 2990 (2022).
4. Smits, R. W. H. et al. Intraoperative assessment of the resection specimen facilitates achievement of adequate margins in oral carcinoma. *Front. Oncol.* 1–9 https://doi.org/10.3389/fonc.2020.614593 (2020).
5. Ballonoff, A., Chen, C. & Raben, D. Current radiation therapy management issues in oral cavity cancer. *Otolaryngol. Clin. North. Am.* **39**, 365–380 (2006).
6. Helliwell, T., Woolgar, J. & Lishman, S. *Standards and Datasets for Reporting Cancers Dataset for Histopathology Reporting of Mucosal Malignancies of the Pharynx* (2013).
7. Schnitt, S. J., Moran, M. S., Houssami, N. & Morrow, M. The Society of Surgical Oncology - American Society for Radiation Oncology consensus guideline on margins for breast-conserving surgery with whole-breast irradiation in stages I and II invasive breast cancer: Perspectives for pathologists. *Arch. Pathol. Lab. Med.* **139**, 575–577. https://doi.org/10.5858/arpa.2014-0384-ED (2015).
8. Faruqi, A. & Rous, B. *Standards and Datasets for Reporting Cancers Dataset for Histopathological Reporting of Vulval Carcinomas Unique Document Number G070 Document Name Dataset for Histopathological Reporting of Vulval Carcinomas* (The Royal College of Pathologists, 2018).
9. Orosco, R. K. et al. Positive surgical margins in the 10 most common solid cancers. *Sci. Rep.* **8**, 5686 (2018).
10. Baddour, H. M., Magliocca, K. R. & Chen, A. Y. The importance of margins in head and neck cancer. *J. Surg. Oncol.* **113**, 248–255 (2016).
11. Aaboubout, Y. et al. Intraoperative assessment of resection margins in oral cavity cancer: This is the way. *J. Vis. Exp.* **171**, e62446 (2021).
12. Barroso, E. M. et al. Performance of intraoperative assessment of resection margins in oral cancer surgery: A review of literature. *Front. Oncol.* **11**, 628297 (2021).
13. Rosenthal, E. L. et al. Safety and tumor specificity of cetuximab-IRDye800 for surgical navigation in head and neck cancer. *Clin. Cancer Res.* **21**, 3658–3666 (2015).
14. Lamberts, L. E. et al. Tumor-Specific uptake of fluorescent Bevacizumab-IRDye800CW microdosing in patients with primary breast cancer: A phase I feasibility study. *Clin. Cancer Res.* **23**, 2730–2741 (2017).
15. Gao, R. W. et al. Safety of panitumumab-IRDye800CW and cetuximab-IRDye800CW for fluorescence-guided surgical navigation in head and neck cancers. *Theranostics* **8**, 2488–2495 (2018).
16. Steinkamp, P. J. et al. A standardized framework for Fluorescence-Guided margin assessment for head and neck cancer using a tumor acidosis sensitive optical imaging agent. *Mol. Imaging Biol.* **23**, 809–817 (2021).
17. de Wit, J. G. et al. EGFR-targeted fluorescence molecular imaging for intraoperative margin assessment in oral cancer patients: A phase II trial. *Nat. Commun.* **14**, 4952 (2023).
18. Sibinga Mulder, B. G. et al. Intraoperative molecular fluorescence imaging of pancreatic cancer by targeting vascular endothelial growth factor: A multicenter feasibility Dose-Escalation study. *J. Nucl. Med.* **64**, 82–89 (2023).
19. Nijboer, T. S. et al. Fluorescence-guided surgery using cetuximab-800CW in patients with penile carcinoma. *BJU Int.* **134**, 268–275 (2024).
20. Voskuil, F. J. et al. Fluorescence-guided imaging for resection margin evaluation in head and neck cancer patients using cetuximab-800CW: A quantitative dose-escalation study. *Theranostics* **10**, 3994–4005 (2020).
21. Noorlag, R., De Bree, R. & Witjes, M. J. H. Image-guided surgery in oral cancer: Toward improved margin control. *Curr. Opin. Oncol.* **34**, 170–176. https://doi.org/10.1097/CCO.0000000000000824 (2022).
22. Voskuil, F. J. et al. Intraoperative imaging in pathology-assisted surgery. *Nat. Biomed. Eng.* **6**, 503–514 (2022).
23. Lazzari, G. et al. Light sheet fluorescence microscopy versus confocal microscopy: in quest of a suitable tool to assess drug and nanomedicine penetration into multicellular tumor spheroids. *Eur. J. Pharm. Biopharm.* **142**, 195–203 (2019).
24. Glaser, A. K. et al. Multi-immersion open-top light-sheet microscope for high-throughput imaging of cleared tissues. *Nat. Commun.* **10**, 2781 (2019).
25. Richardson, D. S. & Lichtman, J. W. Clarifying tissue clearing. *Cell* **162**, 246–257 (2015).
26. Almagro, J., Messal, H. A., Zaw Thin, M., van Rheenen, J. & Behrens, A. Tissue clearing to examine tumour complexity in three dimensions. *Nat. Rev. Cancer* **21**, 718–730 (2021).
27. Kubota, S. I. et al. Whole-Body profiling of cancer metastasis with Single-Cell resolution. *Cell. Rep.* **20**, 236–250 (2017).
28. Takahashi, K. et al. Visualization of the cancer cell cycle by tissue-clearing technology using the Fucci reporter system. *Cancer Sci.* **112**, 3796–3809 (2021).
29. Sabdyusheva Litschauer, I. et al. 3D histopathology of human tumours by fast clearing and ultramicroscopy. *Sci. Rep.* **10**, 17619 (2020).
30. Xie, W. et al. Diagnosing 12 prostate needle cores within an hour of biopsy via open-top light-sheet microscopy. *J. Biomed. Opt.* **25**, 126502 (2020).
31. Kim, J. H. et al. Optimizing tissue-clearing conditions based on analysis of the critical factors affecting tissue-clearing procedures. *Sci. Rep.* **8**, 12815 (2018).
32. Woo, J. et al. Comparative analyses of clearing efficacies of tissue clearing protocols by using a punching assisted clarity analysis. *Front. Bioeng. Biotechnol.* **9**, 784626 (2022).
33. Vulders, R. C. M., van Hoogenhuizen, R. C., van der Giessen, E. & van der Zaag, P. J. Clearing-induced tisssue shrinkage: A novel observation of a thickness size effect. *PLoS One.* **16**, e0261417 (2021).
34. Dong, L., Luiten, G. W., van der Giessen, E. & van der Zaag, P. J. Temporal and Spatial evolution of transparency in tissue clearing. *Biophys. Rev.* **6**, 031401 (2025).
35. Dent, J. A., Polson, A. G. & Klymkowsky, M. W. A whole-mount immunocytochemical analysis of the expression of the intermediate filament protein vimentin in xenopus. *Development* **105**, 61–74 (1989).
36. Yokomizo, T. et al. Whole-mount three-dimensional imaging of internally localized immunostained cells within mouse embryos. *Nat. Protoc.* **7**, 421–423 (2012).
37. Bekkouche, B. M. B., Fritz, H. K. M., Rigosi, E. & O'Carroll, D. C. Comparison of transparency and shrinkage during clearing of insect brains using media with tunable refractive index. *Front. Neuroanat.* **14**, 599282 (2020).
38. van Royen, M. E. et al. Three-dimensional microscopic analysis of clinical prostate specimens. *Histopathology* **69**, 985–992 (2016).
39. Xu, J., Ma, Y., Yu, T. & Zhu, D. Quantitative assessment of optical clearing methods in various intact mouse organs. *J. Biophotonics.* **12**, e201800134 (2019).
40. Zhang, X., Rakesh, K. P., Ravindar, L. & Qin, H. L. Visible-light initiated aerobic oxidations: A critical review. *Green Chem.* **20**, 4790–4803 (2018).
41. McNesby, J. R. & Heller, C. A. Oxidation of liquid aldehydes by molecular oxygen. *Chem. Rev.* **54**, 325–346 (1954).
42. Ueda, H. R. et al. Tissue clearing and its applications in neuroscience. *Nat. Rev. Neurosci.* **21**, 61–79 (2020).

43. Krishnan, G. et al. Fluorescent molecular imaging can improve intraoperative sentinel margin detection in oral squamous cell carcinoma. *J. Nucl. Med.* **63**, 1162–1168 (2022).
44. Wan, P. et al. Evaluation of seven optical clearing methods in mouse brain. *Neurophotonics* **5**, 035007 (2018).
45. Stone, L. D. et al. Interim phase II results using Panitumumab-IRDye800CW during transoral robotic surgery in patients with oropharyngeal cancer. *Clin. Cancer Res.* **30**, 4016–4028 (2024).

Acknowledgements

Author contributions

AF, TSN, BK, FJV, MJHW and PJvdZ contributed to conception and study design. AF, TSN, BK, RMK, BvdV and PJvdZ performed most experiments and conducted most data analysis. AF, TSN, BK, FJV and PJvdZ drafted the manuscript. AF, TSN, BK, RMK, BvdV, MJHW, FJV and PJvdZ revised the manuscript. All authors have seen the manuscript and approved submission.

Declarations

Competing interests

The authors declare no competing interests.

Additional information

Supplementary Information The online version contains supplementary material available at https://doi.org/10.1038/s41598-025-27809-w.

Correspondence and requests for materials should be addressed to P.J.Z.

Reprints and permissions information is available at www.nature.com/reprints.

Publisher's note Springer Nature remains neutral with regard to jurisdictional claims in published maps and institutional affiliations.